Modeling Versatile and Dynamic Anaerobic Metabolism for PAOs/GAOs Competition Using Agent-based Model and Verification via Single Cell Raman Micro-spectroscopy

Guangyu Li [1,2], Nicholas B. Tooker [1], Dongqi Wang [3], Varun Srinivasan [4], James L. Barnard [5], Andrew Russell [6], Beverley Stinson [7], Jim McQuarrie [8], Peter Schauer [9], Adrienne Menniti [9], Erika Varga [10,11], Hélène Hauduc [11], Imre Takács [11], Charles Bott [12], Paul Dombrowski [13], Annalisa Onnis-Hayden [1], and April Z. Gu [2,*]

[1] Department of Civil & Environmental Engineering, Northeastern University, Boston, MA, United States

[2] School of Civil and Environmental Engineering, Cornell University, Ithaca, NY, United States

[3] Department of Municipal and Environmental Engineering, Xi'an University of Technology, Xi'an, Shaanxi, China

[4] Brown and Caldwell, One Tech Drive, Andover, MA, United States

[5] Black & Veatch, Kansas City, MO, United States

[6] South Cary Water Reclamation Facility, Apex, NC, United States

[7] AECOM, Kelowna, BC, Canada

[8] Tetra Tech, Denver, CO, United States

[9] Clean Water Services, Tigard, OR, United States

[10] LISBP, INSA Toulouse, Toulouse, France

[11] Dynamita, Nyons, France

[12] Hampton Roads Sanitation District, Virginia Beach, VA, United States

[13] Woodard & Curran, Inc., CT, United States

[*] Corresponding author email: aprilgu@cornell.edu

ABSTRACT

Side-stream enhanced biological phosphorus removal process (S2EBPR) has been demonstrated to improve performance stability and offer a suite of advantages compared to conventional EBPR design. Design and optimization of S2EBPR require modification of the current EBPR models that were not able to fully reflect the metabolic functions of and competition between the polyphosphate-accumulating organisms (PAOs) and glycogen-accumulating organisms (GAOs) under extended anaerobic conditions as in the S2EBPR conditions. In this study, we proposed and validated an improved model (iEBPR) for simulating PAO and GAO competition that incorporated heterogeneity and versatility in PAO sequential polymer usage, staged maintenance-decay, and glycolysis-TCA pathway shifts. The iEBPR model was first calibrated against bulk batch testing experiment data, being proved to perform better than the previous EBPR model for predicting the soluble orthoP, ammonia, biomass glycogen, and PHA temporal profiles in a batch starvation testing under prolonged anaerobic conditions. We further validated the model with another independent set of batch anaerobic batch testing data that included high-resolution single-cell and specific population level intracellular polymer measurements enabled by the single-cell Raman micro-spectroscopy technique. The model accurately predicted the temporal changes in the intracellular polymers at cellular and population levels within PAOs and GAOs, and further confirmed the proposed mechanism of sequential polymer utilization, and polymer availability-dependent and staged maintenance-decay in PAOs. These results indicate that under extended anaerobic phases as in S2EBPR, the PAOs may gain competitive advantages over GAOs due to the possession of multiple intracellular polymers and the adaptive switching of the anaerobic metabolic pathways that consequently lead to the later and slower decay in PAOs than GAOs. The iEBPR model can be applied to facilitate and optimize the design and operations of S2EBPR for more reliable nutrient removal and recovery from wastewater.

KEYWORDS: EBPR, S2EBPR, Agent-based modeling, Cell maintenance, Cell decay, Glycolysis-TCA pathway switch

INTRODUCTION

The enhanced biological phosphorus removal (EBPR) process has been recommended as a promising strategy to achieve sustainable wastewater P removal and facilitate P recovery (Gu et al., 2018). Current EBPR systems are designed to enrich a key functional group, namely the phosphate-accumulating organisms (PAOs) and *Ca. Accumulibacter phosphatis* is one of the most found PAOs in EBPR systems. Glycogen-accumulating organisms (GAOs) are often observed to coexist with PAOs, who possess a similar glycogen-based VFA-PHA metabolism without the polyphosphate (polyP) storage ability (Oehmen et al., 2006; Zeng et al., 2003) and are therefore concerned to be niche VFA (carbon source) competitors with PAOs consequently impacting EBPR performance. PAO-GAO competition could be kinetically affected by pH, temperature, substrate type, dissolved oxygen, solids retention time (SRT), hydraulic retention time (HRT), feeding strategy (Filipe et al., 2001a; Gu et al., 2008; Lopez-Vazquez et al., 2009; Majed and Gu, 2011; Neethling et al., 2006; Oehmen et al., 2005a, 2005b; Onnis-Hayden et al., 2020a; Rodrigo et al., 1996; Whang et al., 2007), etc. Although the proliferation of GAOs has been associated with EBPR performance deterioration in many cases (Gu et al., 2008; López-V et al., 2007; Oehmen et al., 2007), the coexistence of GAOs presence is not necessarily detrimental to EBPR performance as long as PAOs are kinetically favored (Gu et al., 2018; Nielsen et al., 2019; Onnis-Hayden et al., 2020b).

The performance stability of EBPR has been a concern hindering its wider applications. An emerging technology that has been demonstrated to successfully address the common stability challenge with EBPR is side-stream RAS and mixed liquor hydrolysis/fermentation-based side-stream EBPR (S2EBPR) (Barnard et al., 2010; Copp et al., 2012; Gu et al., 2018; Onnis-Hayden et al., 2020b; Stevens et al., 2015; Stroud and Martin, 2001; Vale et al., 2008; Vollertsen et al., 2006; Wang et al., 2019b). S2EBPR refers to modified EBPR configurations that include a diversion of RAS or anaerobic mixed liquor to a side-stream reactor, where simultaneous VFA production via sludge hydrolysis and fermentation and PAO activity-related P release and carbon uptake occur. Compared to conventional EBPR design, the S2EBPR offers a suite of advantages, including influent-carbon-independent VFA sources for PAO feast, eliminating the influences of fluctuating influent loads, more controllable lower-redox environments, more complex VFA compositions that likely favor the selection of PAOs over GAOs, flexible configurations and potential reduction of carbon footprint and denitrification enhancement by diverting more influent carbon to denitrifiers (Gu et al., 2018; Lanham et al., 2013; Mielczarek et al., 2013; Onnis-Hayden et al., 2020b; Srinivasan et al., 2021; Stokholm-Bjerregaard et al., 2017; Wang et al., 2019b).

While full-scale processes demonstrated the potential promises and advantages of S2EBPR (Barnard et al., 2010; Copp et al., 2012; Onnis-Hayden et al., 2020b; Stevens et al., 2015; Stroud and Martin, 2001; Vale et al., 2008; Vollertsen et al., 2006; Wang et al., 2019b), existing knowledge gaps in the fundamental understanding of the biochemical mechanisms and microbial ecology involved in S2EBPR hampers its wider application and implementation. Design and optimization of S2EBPR require adequate EBPR models that can capture the underlying key mechanisms involved in the S2EBPR such as the VFA production via hydrolysis and fermentation, and PAO and GAO competition in the extended anaerobic side-stream reactor. A few recent modeling efforts failed to predict either this competitive advantage or

88 the performance superiority observed in S2EBPR systems compared to the conventional EBPR systems
89 (Dunlap et al., 2016; Houweling et al., 2010). This suggested that there are still critical aspects in the
90 current EBPR models that cannot reflect the metabolic functions of and competition between the PAOs
91 and GAOs under the S2EBPR conditions, particularly the seemingly more pronounced differential
92 metabolic versatility and dynamics among PAO and GAO subphenotypes under the prolonged anaerobic
93 condition that involve cell maintenance, biomass decay and the associated versatility in the utilization of
94 various intracellular polymers (Guedes da Silva et al., 2020; Lanham et al., 2014; G. Li et al., 2018; Santos
95 et al., 2020).

96 First, PAO and GAO's cell maintenance and cell decay are two processes that are highly relevant in
97 S2EBPR, yet they are not fully understood or accurately modeled in previous EBPR models such as ASM
98 (Henze et al., 2001). Cell maintenance is an observation-driven, hypothesized metabolic process. It was
99 evidenced by continuous consumption of related intracellular polymers in PAO and GAO cells to produce
100 ATP at a constant rate, throughout both short-term (i.e. ≤ 10 hrs) (Filipe et al., 2001a, 2001b; Houweling
101 et al., 2010; Mino et al., 1998; Smolders et al., 1994a; Wentzel et al., 1989; Zeng et al., 2003) and long-
102 term (≥5 days) (Vargas et al., 2013) anaerobic conditions while their known EBPR-related metabolisms
103 are in idle. Previous models (e.g. ASM2 and ASM3+BioP (Henze et al., 2001)) often disregard the
104 constant APT production rate but use a first-order polymer degradation to approximate, potentially
105 causing deviated prediction of polymer consumption in cell maintenance. Evidence from previous
106 literature (Carvalheira et al., 2014; Nielsen et al., 2016) and our recent studies (Gu et al., 2018; Wang et
107 al., 2019b) suggested that the possession and ability of PAOs to utilize both polyP and glycogen offer
108 them competitive advantages over GAOs that rely solely on glycogen, in terms of its survival time length,
109 delayed decay, on-set time, and overall lower decay rates under extended anaerobic conditions as those

110 in S2EBPR processes. This indicates that models such as Barker&Dold and UCTPHO+ (Barker and Dold,
111 1997; Hu et al., 2007), which do not account for the contribution of glycogen in PAO cell maintenance,
112 can potentially underestimate PAOs' competitive advantage. Recent models introduced a *sequential*
113 *polymer usage* strategy to simulate cell maintenance (Lanham et al., 2014; G. Li et al., 2018; Santos et
114 al., 2020) at constant ATP rates, and a *staged maintenance-decay* mechanism to approximate delayed
115 cell decay when PAO and GAO have ample intracellular polymer for maintenance (G. Li et al., 2018;
116 Santos et al., 2020). The previously observed lower-than-expected PAO and GAO decay rates (G. Li et al.,
117 2018; Li et al., 2020; Santos et al., 2020) could potentially be explained by this maintenance survival
118 hypothesis. However, two potential issues remain. First, the preference order of polyP and glycogen
119 consumption is critical in the sequential polymer usage strategy, and both PAO subphenotypes may exist
120 (Lopez et al., 2006; Lu et al., 2007). Conventional population-level models often assume one priority
121 order (usually glycogen-prioritized) and ignore the other (Lanham et al., 2014; Santos et al., 2020),
122 instead of considering both subphenotypes. Second, accurate simulation of cell decay among different
123 PAO subphenotypes depends on the intracellular polymer's availability at the cell level with the staged
124 maintenance-decay strategy, which would be difficult to capture with conventional bulk measurements
125 of aggregated polymer content in the biomass. Validating these proposed mechanisms requires both
126 finer resolution measurements and simulation of the cellular polymer consumption heterogeneity
127 among PAO subphenotypes.

128 Second, both overall microbial community and PAOs diversity in S2EBPR were found to be higher than
129 conventional EBPRs (Onnis-Hayden et al., 2020b; Srinivasan et al., 2021). The recent discoveries pointed
130 to highly varying and versatile anaerobic metabolic strategies among PAO subphenotypes (Guedes da
131 Silva et al., 2020). (Santos et al., 2020) introduced the modeling of pathway switching for better

simulating PAO metabolism. One of the most debated aspects related to the Accumulibacter's anaerobic metabolism is the source of reducing power (NAD(P)H), which is required to reduce VFA into PHA monomers. Early studies suggest glycolysis and tricarboxylic acid (TCA) cycle to be possible sources, resulting in different PAO metabolic models per experimental evidence, including using sole glycolysis (referred to as Mino model) (Mino et al., 1987; Smolders et al., 1994a), sole TCA (referred to as Comeau-Wentzel model, C-W model) (Comeau et al., 1986; Maurer et al., 1997; Wentzel et al., 1989) or a mixture of the two in various ratios (Pereira et al., 1996; Pijuan et al., 2008; Yagci et al., 2003; Zhou et al., 2009). The switch between glycolysis and TCA-oriented metabolisms was hypothesized and implied to be triggered by intracellular polymer availability and depletion (Damir Brdjanovic et al., 1998; Guedes da Silva et al., 2020; Pijuan et al., 2008; Zhou et al., 2009).

In this study, to improve the EBPR model to better predict the S2EBPR processes, we proposed a revised EBPR model that better captures the PAO-GAO competition under extended anaerobic conditions, by incorporating staged maintenance-decay and glycolysis-TCA pathway shifts that are linked to the heterogeneity and versatility of PAO metabolism involving dynamic intercellular polymers usage. In addition, we employed an agent-based model to overcome the limitations in the current EBPR model that cannot capture the evidenced higher diversity of PAOs in S2EBPR than conventional EBPR (Srinivasan et al., 2021). The higher phylogenetic and phenotypic diversity of PAOs in the S2EBRP system compared to the conventional systems (Srinivasan et al., 2021; Wang et al., 2019b) likely resulted from more complex substrates and higher anaerobic SRT in the side-stream reactors and, they play a key role in the mechanisms underlying the PAO-GAO competition in S2EBPR. Agent-based modeling can capture the detailed PAO-GAO competition that involves the heterogeneity of subphenotypes (Y. Li et al., 2018; Majed et al., 2009; Majed and Gu, 2020, 2010) beyond those evaluated at aggregated and bulk

154 estimates as in most previous studies (Guedes da Silva et al., 2020; Lopez-Vazquez et al., 2009).
155 Furthermore and most importantly, we experimentally verified the proposed model with observations
156 on cell-level, quantitative polymer dynamics by leveraging the power of single-cell Raman micro-
157 spectroscopy technology (Bucci et al., 2012; Majed et al., 2009; Majed and Gu, 2011). To our knowledge,
158 this was the first-time effort to verify the improved metabolic model using experimentally obtained
159 single-cell intracellular polymer measurements from full-scale S2EBPR systems. The proposed model,
160 referred to as iEBPR, outperformed the previous model in predicting the experimentally observed trends
161 of intracellular polymer biomass content under anaerobic conditions and was proven to be more
162 effective in simulating PAO and GAO maintenance behavior under those extended anaerobic conditions
163 than conventional models. The proposed mechanism can be incorporated into future EBPR models to
164 reveal the overall EBPR performance and PAO-GAO competitive dynamics more accurately as observed
165 in S2EBPR systems.

166

167 **METHODOLOGY**

168 **Agent-based EBPR Model Structure**

169 An agent-based EBPR model (named iEBPR) was developed based on our previous iAlgae model
170 developed by (Bucci et al., 2012). In this study, three population groups were included, namely PAOs,
171 GAOs, and OHOs. OHOs stand for ordinary heterotrophic organisms that account for all non-PAO and
172 non-GAO species. The same fundamental metabolic framework in iAlgae was used, including
173 Accumulibacter-PAOs and OHOs taken from the International Water Association's Activated Sludge

Model 2 (ASM2) (Henze et al., 2001), and Competibacter-like GAOs coded for anaerobic VFA-uptake, PHA synthesis and aerobic biomass growth PHA-degradation and glycogen-accumulation (Filipe et al., 2001b; Houweling et al., 2010; Zeng et al., 2003). Note that iAlgae simplified VFAs to acetate and PHAs to PHB, which were kept in iEBPR and similar to (Santos et al., 2020). In addition, this study focused on PAO-GAO competition under extended anaerobic conditions; and denitrifiers, nitrifiers, and other anoxic-related organisms were not included. Similar to iAlgae, the inert organic matter was not tracked, and released matter from cell lysis would instantly transform into rbCOD (VFA) (Bucci et al., 2012) assuming the hydrolysis of inert organic matter is instant. The Gujer matrices of PAO, GAO, and OHO are shown in **Table S1-3**.

Representation of population phenotype heterogeneity. Each modeled species, i.e. PAO, GAO, or OHO was simulated in 10,000 independent agents known as the approach of agent-based modeling. Agents have independent polymer and biomass values and randomly assigned kinetic parameters to approximate metabolic heterogeneity among subphenotypic groups as in real activated sludge. Stoichiometric (yield) parameters were theoretically determined and were not randomized. Kinetic parameters, including rates and affinity parameters, were randomized by normal distributions, with their means representing the bulk-level aggregated values (for calibration to data, using literature values (Filipe et al., 2001b; Lopez-Vazquez et al., 2009; Zeng et al., 2003) or ASM2 defaults (Gujer, 1994)), and standard deviations for calibration. Invalid and exotic values (e.g. negative rates) from randomization were discarded and regenerated. In agent-based modeling, the number of agents is an important parameter to balance between simulating heterogeneity and computational time. We found that 1,000-10,000 agents per species were adequate considering this trade-off. In addition, all agents were updated

synchronously at the end of each elapsed time step, known as the *discrete-event simulation* (Kurve et al., 2013).

Polymer Availability-dependent Agent-level Energy Derivation for Cell Maintenance and Decay

Based on the fundamental metabolic framework from iAlgae, sequential polymer usage and staged maintenance-decay process were incorporated to replace the first-order decay mechanism. Unlike the population-level models in previous studies (Lanham et al., 2014; Santos et al., 2020), this calculation was performed at the agent level, allowing heterogenic cell maintenance and decay concerning the heterogeneity in polymer storage.

Cell maintenance with flexible and sequential polymer usage. PAO and GAO cell maintenance were simulated to fulfill a targeted ATP production rate, denoted as m^{ATP}, expressed in mol-ATP/(C-mol biomass.hr). The equivalent polymer consumption rates to generate this ATP (in mg polyP-P/(mg biomass COD.day) and mg glycogen-COD/(mg biomass COD.day)) were calculated based on known stoichiometry and yield coefficients reported in the previous studies (Filipe et al., 2001b; Lu et al., 2007; Smolders et al., 1994a; Zeng et al., 2003). When the polymer(s) are ample, the actual maintenance is hypothesized to achieve the targeted rate (m^{ATP}) without surplus; when polymer(s) are depleted, insufficient cell maintenance will occur and cause cell decay. This calculation is followed by both PAO and GAO biomass. In addition, as PAO has two polymers utilizable for cell maintenance, sequential polymer usage calculation is further incorporated to determine the individual ATP contribution from glycogen and polyP respectively. (Lanham et al., 2014) and (Santos et al., 2020) showed an example of this sequential usage calculation assuming using polyP prior to glycogen:

$$r_{polyP} = M_{polyP} m^{ATP}$$

$$r_{glycogen} = M_{glycogen}\left(m^{ATP} - r_{polyP}\right)$$

215 , where: r_{polyP} and $r_{glycogen}$ are the per polymer ATP contribution; m^{ATP} is the target cell-maintenance
216 rate; M_{polyP} and $M_{glycogen}$ are Monod functions as rate modifiers based on per-polymer utilization
217 affinity and availability. In this study, the other glycogen-preferring phenotype was also included

$$r_{glycogen} = M_{glycogen} m^{ATP}$$

$$r_{polyP} = M_{polyP}\left(m^{ATP} - r_{glycogen}\right)$$

218 , for enabling more flexibly simulating of the observed cases in various studies (Lopez et al., 2006; Lu et
219 al., 2007; Vargas et al., 2013). The selection of polyP-glycogen priority is designed to be a calibratable
220 parameter.

221 ***Staged and linked cell maintenance and decay.*** Previous EBPR models considered cell decay as an
222 intrinsic process at a constant specific rate i.e., first-order decay, and as a process independent of cell
223 maintenance. Several studies have shown evidence of accelerated biomass decay after depletion of
224 their intracellular polymers. Since cell maintenance consumes polymers, this implies a linkage between
225 biomass decay and cease of maintenance (Lu et al., 2007; Vargas et al., 2013). In our previous work (G. Li
226 et al., 2018), we first introduced the process to link these two processes, hypothesizing that cells will
227 aim to use the intracellular polymer(s)-derived energy for maintenance first to survive, before initiating
228 decay when the energy can no longer satisfy the need for maintenance. Briefly, we treat the proportion

of insufficient cell maintenance as the switch function to enable cell decay, making the PAO and GAO agents avoid decaying when their polymers are ample for cell maintenance, and start decaying when depleted:

$$b_r = b_{max}\left(1 - \frac{r^{ATP}}{m^{ATP}}\right)$$

, where: b_r is the actual specific decay rate; b_{max} is the maximum specific decay rate. The formulation took into consideration of mathematical simplicity. The decayed biomass then proportionally regenerates as rbCOD (VFA) based on the empirical PAO/GAO biomass formula $CH_{1.93}O_{0.53}N_{0.2}$ (Zeng et al., 2003). Although ammonia release was not direct tracked in the model, it could still be estimated using the above empirical biomass formula, which could be compared with experimental ammonia measurements used as an indicator of biomass decay (Lu et al., 2007). Linking cell maintenance to cell decay effectively models cell maintenance as an endogenous metabolic process that "precedes and inhibits" cell decay, making it a "survival strategy" for PAO and GAO species (Santos et al., 2020).

Agent-level Glycolysis and TCA Cycle Pathway Switching

Based on our current knowledge, PAO's glycolysis-oriented PHA synthesis will cease upon glycogen depletion, then the TCA-oriented PHA synthesis can continue as it doesn't require glycogen (Guedes da Silva et al., 2020; Yagci et al., 2003; Zhou et al., 2009). The C-W model was chosen (Comeau et al., 1986; Wentzel et al., 1989) as the representative stoichiometry of TCA-oriented metabolism for its wide adoption in other EBPR models. The Mino model (Mino et al., 1998; Smolders et al., 1995) was used as the glycolysis-oriented stoichiometry. Note that both the Mino model and C-W model require the presence of polyP for PAO's anaerobic PHA synthesis, making the same restriction in iEBPR. This

implies that iEBPR does not allow GAO-like, polyP-independent metabolism in PAO cells, though it is still controversial in observation (Acevedo et al., 2012; Guedes da Silva et al., 2020). Furthermore, the glycolysis-oriented pathway was assumed to be prioritized due to its higher carbon efficiency than the TCA-oriented PHA synthesis (Guedes da Silva et al., 2020). To model the leveraged PHA synthesis rate, the following modifications are applied:

$$q_{PHA,glycogen} = M_{glycogen} M_{other} q_{PHA}$$

$$q_{PHA,TCA} = s\left(1 - M_{glycogen}\right) M_{other} q_{PHA}$$

, where $q_{PHA,glycogen}$ and $q_{PHA,TCA}$ are the adjusted PHA synthesis rates contributed by glycolysis-oriented and TCA-oriented metabolism respectively; $M_{glycogen}$ is the Monod function related to glycogen availability; M_{other} is an aggregated term of other applicable rate modifiers used in ASM2; and q_{PHA} is intrinsic PHA synthesis rate. The combined effect of these two PHA synthesis rates can simulate the employment of these two metabolism pathways in various degrees observed in previous studies (Comeau et al., 1986; Hesselmann et al., 2000; Lanham et al., 2013; Maurer et al., 1997; Mino et al., 1998; Pereira et al., 1996; Pijuan et al., 2008; Smolders et al., 1995; Wentzel et al., 1989; Yagci et al., 2003; Zhou et al., 2009). The binary parameter s (possible values are 0 and 1) is a phenotype indicator, for which 1 indicates an agent that can switch from glycolysis to TCA-oriented metabolism and 0 for being restricted to glycolysis-only. The relative abundance of agent subphenotypes can represent the relative abundance of PAO subphenotypes in real sludge, which enables the simulation of the coexistence and competition between these two subphenotypes. To our knowledge, this feature is exclusive to agent-based modeling and iEBPR is the first model to incorporate this into EBPR modeling.

iEBPR Model Calibration

iEBPR was first calibrated with a set of data retrieved from a previous 8-day anaerobic starvation study in a lab-scale Accumulibacter-enriched (~85% reported abundance) EBPR system (Lu et al., 2007). The initial contents of glycogen, PHA, and polyP were derived from the above literature using the empirical PAO biomass formula $CH_{1.93}O_{0.53}N_{0.2}$ (Zeng et al., 2003). Gradient descent was used to automate the calibration of PAO and GAO anaerobic kinetic parameters. Briefly, the root mean square errors (RMSEs) of PHA, glycogen, orthoP, and MLVSS lysis (estimated by NH_4^+-N release) were calculated respectively; their geometric mean was used as the aggregated loss function (error measure). Geometric mean was used rather than arithmetic mean to arise the sensitivity of MLVSS lysis (NH_4^+-N release), which is two-magnitude smaller than orthoP. The calibration process takes a randomly generated parameter set as the start point and keeps adjusting the parameter values by small steps to reduce RMSE until no better parameter set can be found nearby (i.e. reached local minimum). Since local minima are sensitive to the initial parameter set, the above process was repeated 10,000 times with random initialization, and the best result was considered as the optimized parameter set. Other coefficients not subject to this calibration such as yields, were set the values from previous studies or the ASM2 model defaults (Lopez-Vazquez et al., 2009; Smolders et al., 1994b; Zeng et al., 2003). **Table S4-6** shows the final parameter set for PAOs and OHOs respectively, and unit conversions are shown in **Note S7**. The performance of the iEBPR model with calibrated parameter set was compared to conventional EBPR (calibrated separately).

Cellular-level Experimental Observations via Single-cell Raman Micro-spectroscopy for Model Verification

286 Previous studies proposed single-cell Raman micro-spectroscopy (SCRS) to be a promising technology in
287 estimating the glycogen, PHA, and polyP in individual cells, to further reveal the polymer distributions at
288 both cellular and population levels (Y. Li et al., 2018; Majed et al., 2009; Majed and Gu, 2020, p. 20,
289 2010). This phenotypic survey data is comparable with the polymer distribution predicted by agent-
290 based modeling (Bucci et al., 2012).

291 ***SCRS dataset acquisition.*** An SCRS dataset was first acquired individually for each sludge sample based
292 on the method detailed in previous studies (Gu et al., 2018; Majed et al., 2009; Majed and Gu, 2011;
293 Wang et al., 2019a). Briefly, 1 mL of MLSS was washed twice with 0.9% (w/v) NaCl solution and
294 homogenized by passing in and out of a 26-gauge needle and syringe for at least 20 times to obtain
295 uniform distribution of cells, as described previously. Then 6-8 drops of the disrupted sample were
296 spread and dried on aluminum-coated slides (EMF Corp., Ithaca, US). After that, the slide was dipped
297 into ice-cold Milli-Q water several times to remove salt particles and dried with filtered nitrogen gas. For
298 each sample, Raman spectra for at least 80 single cells were acquired using a multiline confocal Raman
299 spectrometer (LabRam HR Evolution, Horiba Jobin Yvon, Kyoto, Japan) configured with a 532 nm Nd:YAG
300 laser and a 600 gr/mm grating. A 100× long working distance objective with a numerical aperture (NA)
301 of 0.9 and a working distance of 0.21 mm was used to observe and collect Raman signals from single
302 cells. The acquisition time for each spectrum was 20 seconds per cell and the laser power was set to
303 10%. Spectra were collected with scans from 400 cm^{-1} to 1800 cm^{-1}.

304 ***SCRS data processing.*** Raman spectra processing and polymer relative abundance calculation were
305 detailed in previous studies (Gu et al., 2018; Majed et al., 2009; Majed and Gu, 2011; Wang et al.,
306 2019a). All Raman spectra were processed using cosmic spike removal, smoothing, background
307 subtraction, and baseline correction using LabSpec 6 software (Horiba Jobin Yvon, Kyoto, Japan). Quality

308 control was conducted by excluding the spectra showing unexpected signals (damaged) or low SNR, or
309 lack of major characteristic peaks from bacterial components such as phenylalanine (~1002 cm^{-1}) and
310 amide I (~1657 cm^{-1}). The candidate PAO and GAO populations were quantified based on the different
311 combinations of intracellular polymeric inclusions, including poly-P (band at 690-700 cm^{-1} for P-O-P
312 vibrations and band at 1168-1177 cm^{-1} for PO_2^- stretching band), PHAs (bands at ~434 cm^{-1},~839 cm^{-1},
313 and ~1723 cm^{-1}), and glycogen (bands at ~480 cm^{-1},~852 cm^{-1}, and ~938 cm^{-1}), as described previously
314 (Majed and Gu, 2020). The relative content of poly-P, PHAs, and glycogen in each candidate PAO and
315 GAO cell were evaluated based on the intensity of the bands at 1168-1177 cm^{-1}, ~1723 cm^{-1}, and ~480
316 cm^{-1}, respectively (normalized against the intensity of the amide I band). The polymer distribution in
317 PAO and GAO species was then estimated based on the polymer relative abundances within PAO and
318 GAO candidate cells collected in each sample respectively.

319

320 **RESULTS AND DISCUSSION**

321 **iEBPR Model Calibrations against Anaerobic Starvation Batch Testing Results**

322 iEBPR was calibrated against the temporal profile of orthophosphate and residual ammonia
323 concentration and bulk measurements of intracellular glycogen and PHA using data extracted from (Lu
324 et al., 2007, p. 200) (**Figure 1, Table 1**). The results showed that the sequential polymer usage and
325 staged maintenance-decay as incorporated by the iEBPR performed quantitatively better than
326 iAlgae/ASM2, in predicting the temporal profiles of orthoP release, cell lysis (NH_4^+-N release), glycogen,
327 and PHA. Based on the experimental observations (**Figure 1**), the 8-day anaerobic starvation could be

328 divided into 4 phases: (1) Glycogen degradation phase featuring fast glycogen reservoir depletion within
329 the first day, accompanied by corresponding quick PHA formation and a relatively small amount of P
330 release from polyP consumption; (2) Accelerated polyP consumption and P release, coupled with
331 continuous glycogen degradation until its depletion. The majority of PHA accumulation (>90%) was done
332 by the end of this phase in comparison to the final value observed at the end of this 8-day testing. The
333 biomass (85% PAO) decay was also slight in this phase; (3) Deceleration of phosphate release indicated
334 the slowing-down utilization of polyP, likely due to its near-depletion. The acceleration of NH_4^+-N release
335 also indicated a transition of PAO endogenous metabolism and a starting of cell lysis. The acceleration
336 then deceleration of orthoP release from Phase (1)-(3) resembled an S-shaped curve of orthoP
337 concentration profile (**Figure 1**), indicating a transition in ATP source from glycogen to polyP based on
338 glycogen availability. This transition was predicted by iEBPR but not by iAlgae/ASM2 which lacks the key
339 mechanisms, such as sequential polymer usage.

340 **Figure 2** shows the detailed ATP productions suggesting a preference for glycogen priority over polyP for
341 cell maintenance in this sludge. This was accompanied by the transition from glycogen-oriented to
342 polyP-oriented cell maintenance, combined to achieve a cell maintenance rate at 2.1×10^{-3} mol
343 ATP/(C-mol VSS·hr), which was comparable with values from other studies (**Table 1**). Calibration also
344 suggested that only a very small portion of PAOs (< 1%) can switch to TCA-oriented PHA synthesis in this
345 particular sludge, in agreement with the results found in the original experiment where no significant
346 PHA formation was observed after glycogen depletion (Lu et al., 2007).

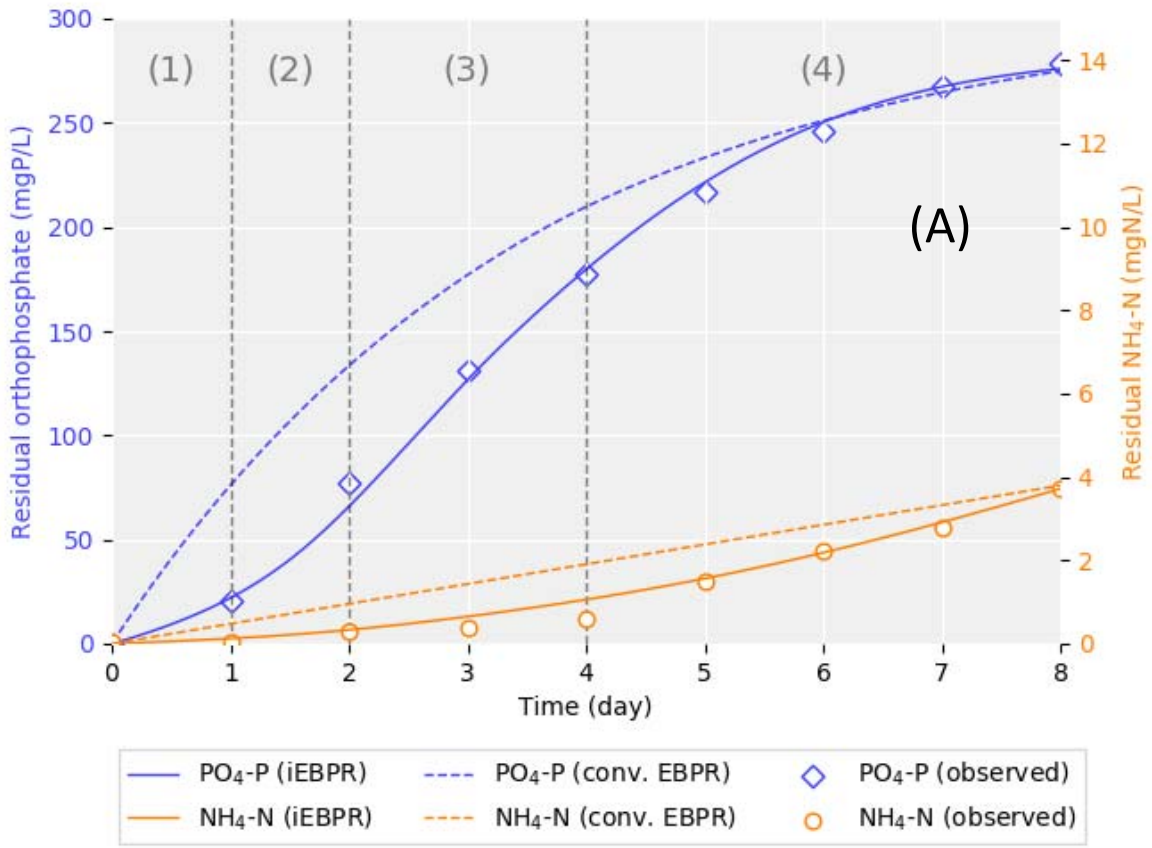
(1)
(2)
(3)
(4)
(A)
Residual orthophosphate (mgP/L)
Residual NH4-N (mgN/L)
Time (day)
PO4-P (iEBPR)
PO4-P (conv. EBPR)
PO4-P (observed)
NH4-N (iEBPR)
NH4-N (conv. EBPR)
NH4-N (observed)

347

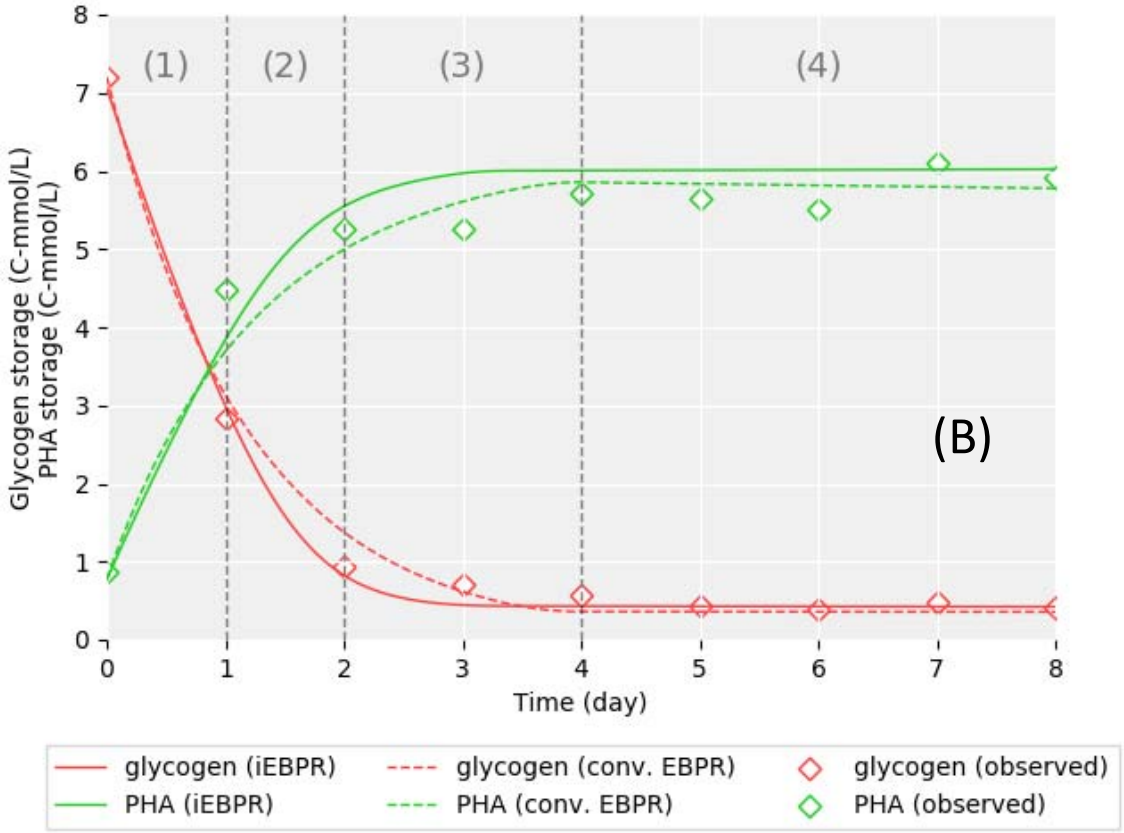

Figure 1. Model comparison between iEBPR and conventional EBPR in predicting the temporal profile of (A) orthoP and NH_4^+-N (cell decay indicator), and (B) intracellular glycogen and PHA, with experimental data acquired from an acetate-fed lab-scale EBPR system with approximately 85% Accumulibacter-PAOs during an 8-day anaerobic starvation batch test by (Lu et al., 2007). Time phases (1)-(4) indicate the four stages observed during the batch test: (1) rapid glycogen degradation; (2) transition stage from glycogen to polyP; (3) polyP utilization; and (4) polyP depletion stage with on-set of significant NH_4^+-N release (cell lysis).

356 **Table 1.** Modeling accuracy comparison in root mean square error (RMSE) between iEBPR and conventional
357 EBPR (iAlgae/ASM2). Observation data was acquired from an 8-day anaerobic starvation test of an acetate-
358 fed PAO-enriched (about 85%) lab-scale sludge by (Lu et al., 2007).

Model	RMSE			
	PO_4-P	NH_4^+-N	PHA	Glycogen
	mgP/L	mgN/L	C-mol/L	C-mol/L
iEBPR* (this study)	5.98	0.18	0.34	0.12
iAlgae/ASM2(Bucci et al., 2012; Henze et al., 2001)	33.0	1.08	0.34	0.19

359 * Improved with staged maintenance-decay, sequential polymer usage in anaerobic cell maintenance, and
360 glycolysis-TCA pathway switching.

361

362 ***Sequential polymer usage predicted PAO-GAO competition more accurately.*** Sequential polymer usage
363 proposed a correction to the overestimation of anaerobic PAO intracellular polymer degradation. In
364 comparison to the iAlgae which uses first-order decay kinetics, iEBPR estimated significantly less polyP
365 degradation in the first three days during the batch testing (**Figure 1A**). The first-order polyP usage (used
366 by iAlgae/ASM2) in cell maintenance failed to reflect the observed ATP production transition from

367 glycogen to polyP-dependent, resulting in excessive polyP degradation when glycogen was still ample.
368 The maximum polyP degradation overestimation was around 56 mgP/L in comparison to the
369 observation data at the end of day 2 (**Figure 1**). This overestimation could significantly underestimate
370 the PAO's competitive advantage against GAO, particularly in the first 24 hrs. This could potentially
371 explain the reason for conventional models like ASM2 to underestimate full-scale S2EBPR performances
372 where prolonged anaerobic conditions are more relevant. A dedicated sequential polymer usage can
373 therefore correct this overestimation and predict PAO anaerobic competition advantages more
374 accurately.

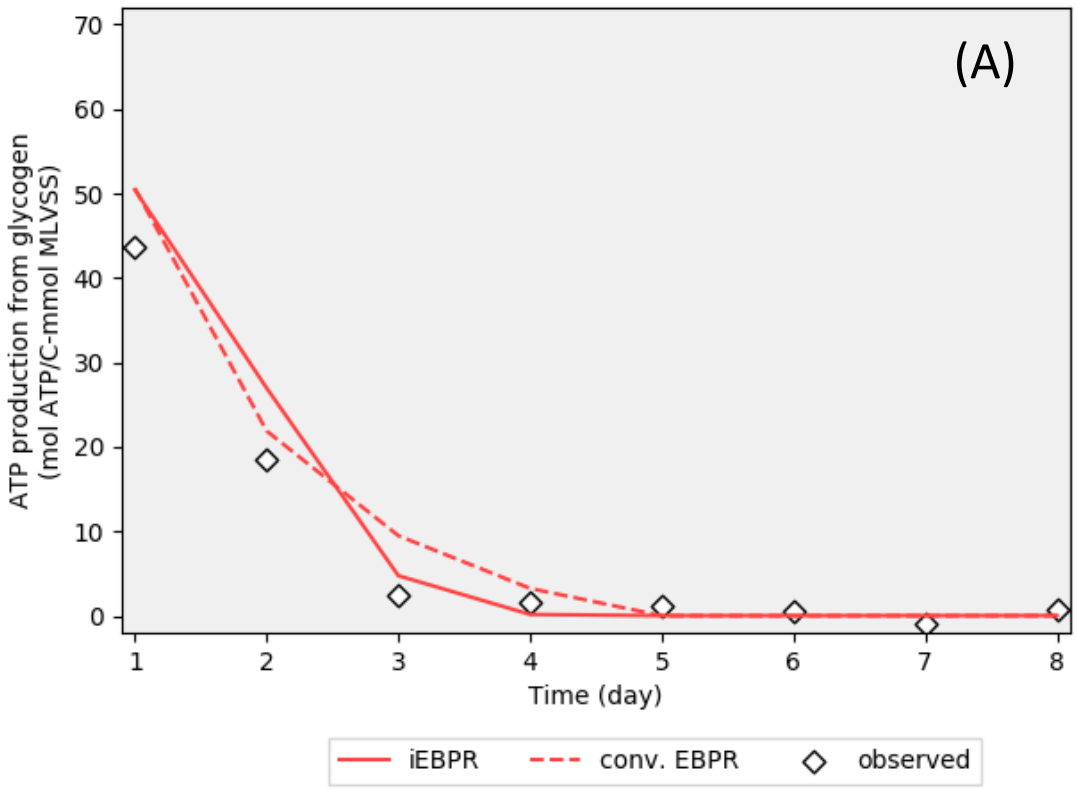

375

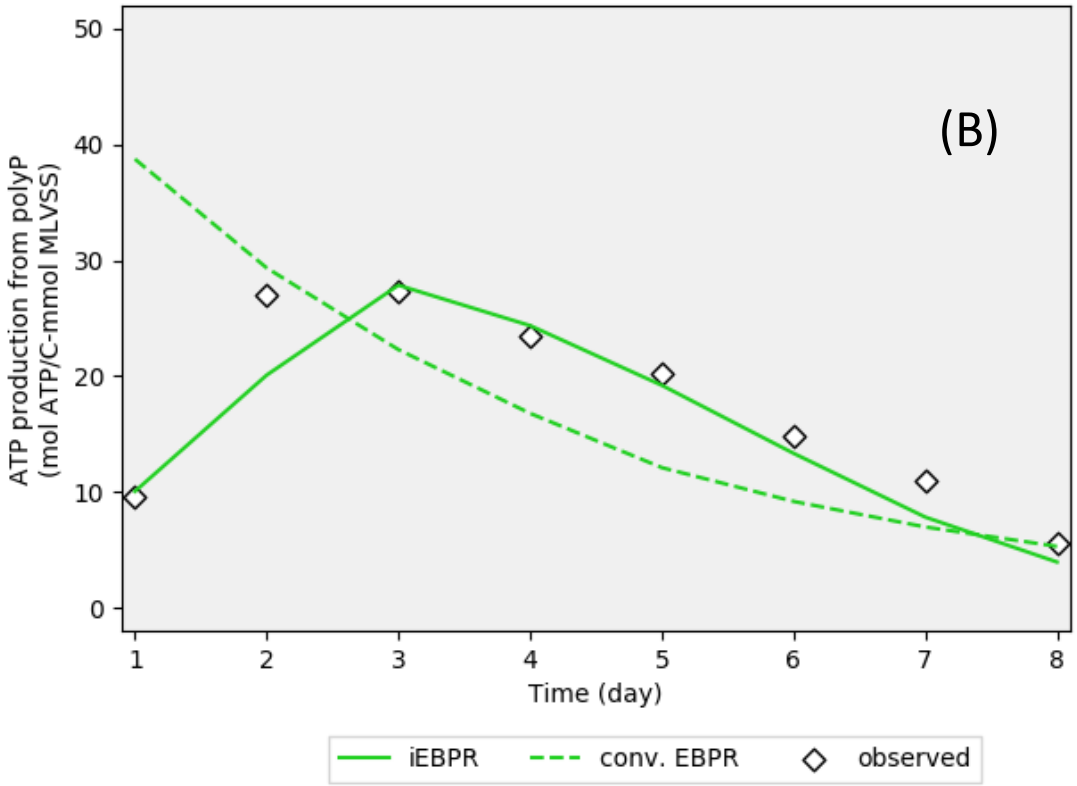

Figure 2. Comparison of model predictions and experimental observations of glycogen-contributed (A) and polyP-contributed (B) ATP during an 8-day anaerobic starvation testing with acetate-fed lab-scale EBPR system containing about 85% as Accumulibacter-PAOs (used as calibration dataset) by (Lu et al., 2007). The iEBPR developed in this study is designed with sequential anaerobic maintenance polymer usage, staged maintenance-decay, and glycolysis-TCA pathway switch; conventional EBPR (iAlgae/ASM2 (Bucci et al., 2012; Henze et al., 2001)) uses the same first-order decay.

Staged maintenance-decay predicted PAO-GAO competition more accurately. The staged maintenance-decay mechanism predicted more accurate cell decay kinetics, indicating an improved PAO anaerobic competitive advantage in comparison to first-order cell decay in iAlgae/ASM2 (**Figure 1&2,**

386 **Table 1**) The observation data showed an acceleration in NH_4^+-N release at the end of day 4, which is
387 adopted by other studies as a cell lysis indicator (Gujer, 1994; Lu et al., 2007). iEBPR could account for
388 this acceleration using the hypothetical staged maintenance-decay mechanism, as shown in **Figure 1**.
389 The calibrated PAO specific decay rate was 0.007/d, close to the reported value of 0.006/d from the
390 literature. In comparison, iAlgae/ASM2 using conventional first-order decay cannot come up with a
391 parameter value to comply with both short-term and long-term NH_4^+-N release predictions. For long-
392 term (at the end of day 8) fit, a decay rate of 0.0028/d had to be used. Despite that this value was 53%
393 below the literature value of 0.006/d, it caused a significant NH_4^+-N release overprediction of 1.91mg/L
394 on day 4 (**Figure 1**) at the same time due to the assumption of always-occurring cell lysis implied by the
395 first-order decay. In comparison, the relevant iEBPR prediction was 0.89mg/L, being much closer to the
396 observed value of 0.60mg/L. Therefore, using more detailed cell decay kinetics, such as staged
397 maintenance-decay could be crucial to improving the model performance and accuracy to simulate
398 S2EBPR systems that have extended anaerobic incubation SRT.

399 **iEBPR Model Validation Case Study: Simulating PAO and GAO Competition under Extended Anaerobic**
400 **Incubation Using Full-scale S2EBPR Sludge**

401 ***Model prediction at the bulk level.*** The calibrated model was then used to simulate an independent
402 anaerobic incubation batch testing similar to the conditions in the side-stream reactor in S2EBPR
403 systems (Gu et al., 2018). The testing sludge was sampled from the side-stream fermentation reactor (in
404 SSR configuration) of the South Cary Water Reclamation Facility (Apex, North Carolina) as described by
405 (Gu et al., 2018) and (Onnis-Hayden et al., 2020a). It was estimated to contain 6.9% biovolume as
406 Accumulibacter-PAOs and 1.1% as known GAOs by fluoresces *in situ* hybridization (FISH) (Gu et al.,
407 2018). The model results were compared against the results from the batch tests that were conducted

408 as a 72-hr anaerobic incubation without external VFA feeding, and the residual orthoP, residual VFA,
409 MLSS glycogen, and PHA were monitored and measured at 0, 6, 12, 18, 24, 36 and 72 hours since the
410 beginning of this incubation. The model was fitted to these temporal profiles with adjustment on the
411 PAO/GAO/OHO composition, polymer contents, and the proportion of glycolysis-TCA switchable PAO
412 phenotype. In addition, OHOs' cell decay rate was also adjusted to the experimentally identified value.
413 All other kinetic and stoichiometric parameters were set identical to the lab-scale sludge calibration
414 results as described above in the previous section without further calibrations. GAO's kinetic and
415 stoichiometric parameters were set identical to PAO's except for the yield ratio of PHA from VFA uptake,
416 for which literature value derived from their glycogen-only metabolism was used (Lopez-Vazquez et al.,
417 2009; Zeng et al., 2003).

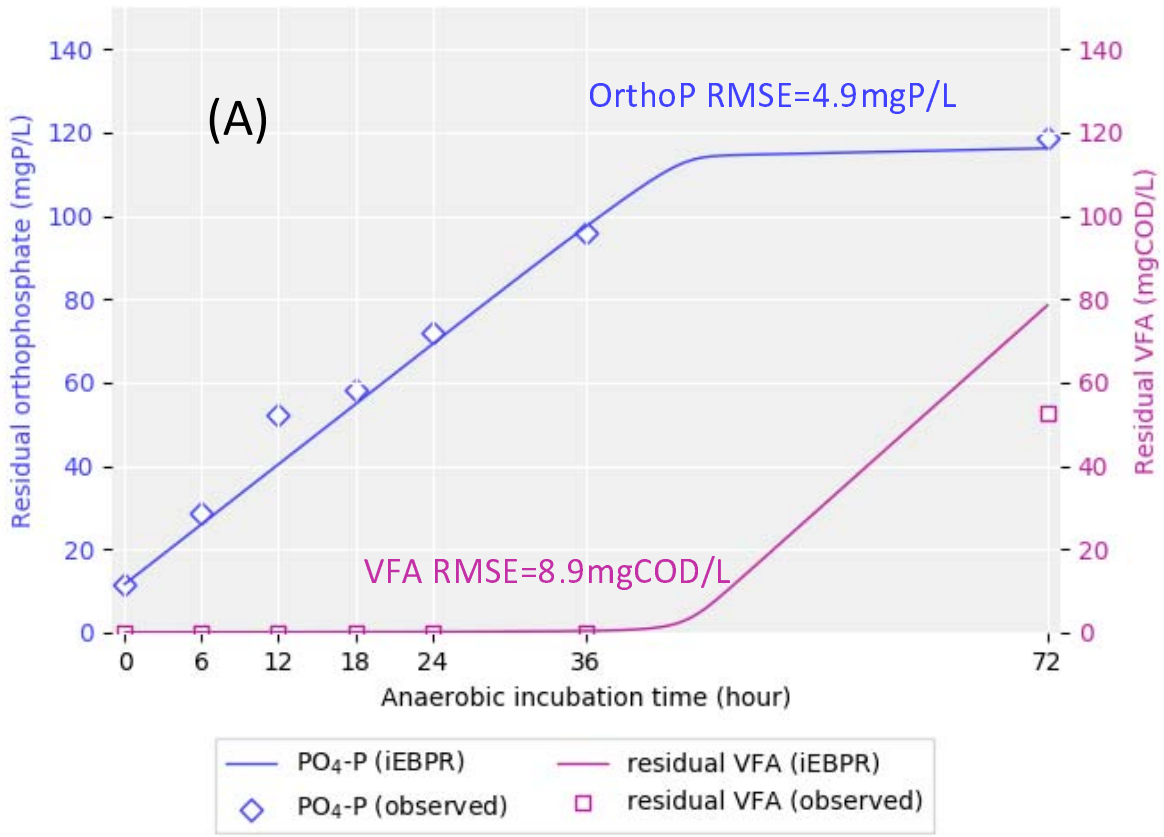
(A)
OrthoP RMSE=4.9mgP/L
VFA RMSE=8.9mgCOD/L
Residual orthophosphate (mgP/L)
Residual VFA (mgCOD/L)
Anaerobic incubation time (hour)
0
6
12
18
24
36
72
0
20
40
60
80
100
120
140
PO4-P (iEBPR)
PO4-P (observed)
residual VFA (iEBPR)
residual VFA (observed)

418

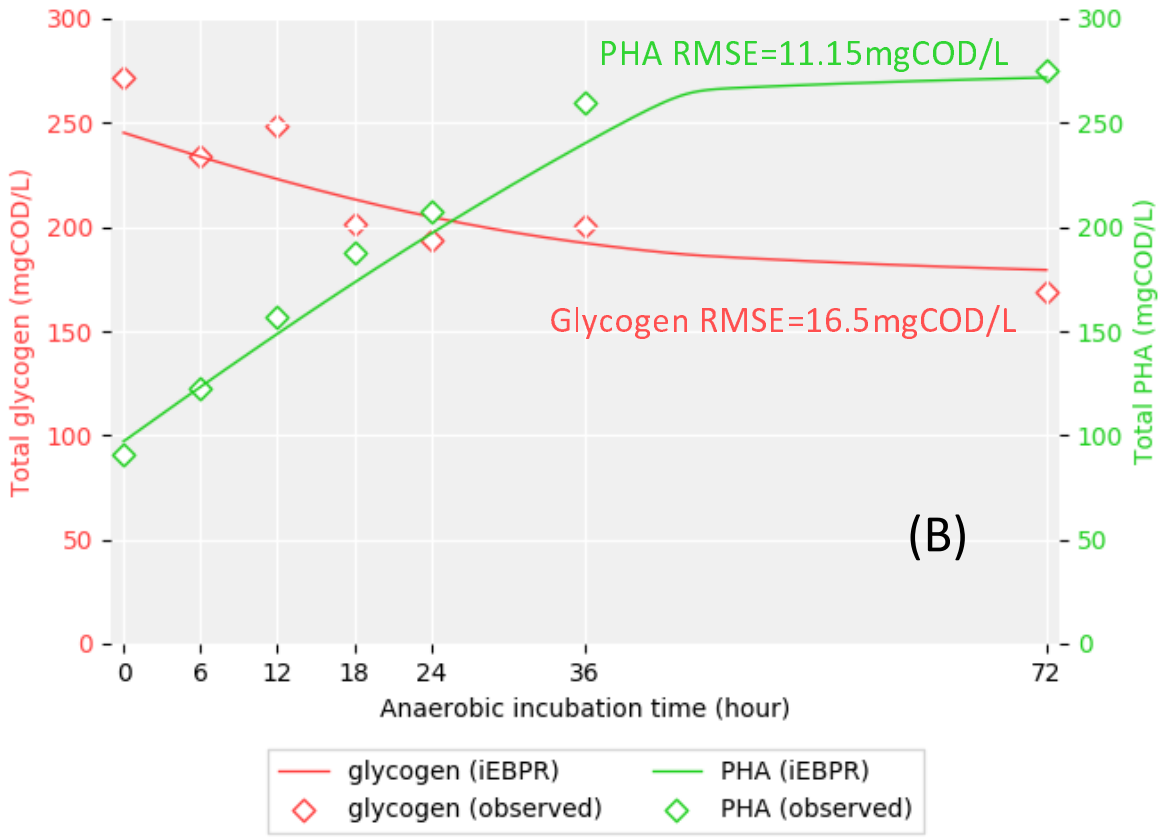

Figure 3. iEBPR simulation results of (A) residual orthoP and residual VFA, and (B) intracellular PHA and intracellular glycogen temporal profile in comparison to the experimental observations in a 72-hour anaerobic incubation batch testing. The tested activated sludge was sampled from a full-scale S2EBPR system (SSR configuration, South Cary WRF, Apex, NC), containing 6.9% as Accumulibacter-PAO, 1.1% as GAOs (estimated in biovolume by FISH). iEBPR incorporates three improved mechanisms: sequential polymer usage in cell maintenance, staged maintenance-decay, and PAO glycolysis-TCA pathway switch, all designed for S2EBPR-like extended anaerobic incubations.

Figure 3 shows that the observed bulk measurements agreed well with the predicted temporal profiles of residual orthoP, residual VFA, total intracellular PHA, and glycogen during the anaerobic batch testing

429 with S2EBPR sludge. The OHO decay rate was calculated to be 0.0076/d based on the VFA requirement
430 to fit observed anaerobic metabolism, balanced by the stoichiometry of P release, glycogen
431 consumption, and PHA formation. The model predicted a transitioning at around 45 hours from the
432 high-rate active P release coupling a significant PHA synthesis phase to the second phase with a slower
433 increase in both PHA and residual P. Calculated yield ratio of the active P release to PHA formation from
434 0-36 hours was 1.16 mol-P/C-mol PHA, which is comparable and within the range of 0.78-1.22 mol-P/C-
435 mol PHA reported for S2EBPR sludge (Lanham et al., 2013) and it is higher than the typical range 0.36-
436 0.77 mol-P/C-mol PHA for conventional A/O enriched sludge (Filipe et al., 2001a; Hu et al., 2007;
437 Smolders et al., 1994a; Yagci et al., 2003). This high orthoP release is likely related to PAO metabolism as
438 the orthoP release transition correlated with PHA formation, and potentially calls for adjustments and
439 updates to the conventional PAO PHA synthesis stoichiometry for S2EBPR alike conditions. Overall,
440 these bulk-level assessments demonstrated the general agreement of the model with mixture culture-
441 level observations, though more detailed insights into the polymer fate and distribution at population
442 and cellular levels that better reflect the competition between PAOs and GAOs could not be deduced.

443 ***Model prediction at the cell group level.*** The capability of inspecting intracellular polymer distribution at
444 cell group resolution provided by the agent-based model enables an explicit way to further validate the
445 proposed mechanisms related to polymer-dependent maintenance and staged maintenance-decay.
446 SCRS was employed to measure and reveal the dynamics of intracellular polymers in PAOs and GAOs
447 that ultimately dictate their competition, and they were compared against the agent-based model
448 results. The initial distributions of PAOs' and GAOs' intracellular polymers, namely polyP and glycogen in
449 PAOs and glycogen in GAOs, were fitted to the observed distribution following (Bucci et al., 2012)
450 protocol. The model predicted polymer distributions were summarized from the agent polymer contents

at 0, 6, 12, 24, 36, and 72 hours, and were compared with the SCRS observations at respective time points (Y. Li et al., 2018; Majed et al., 2009; Majed and Gu, 2010). The comparison between the model-predicted distributions against RCRS observations were shown in **Figure 4**. The accurate prediction of the EBPR-related intracellular polymer distribution changes indicates that the agent-based simulation in iEBPR can effectively track those polymer dynamics, emphasizing that our proposed maintenance-delay mechanism can be applied at the cell-group level and resolution.

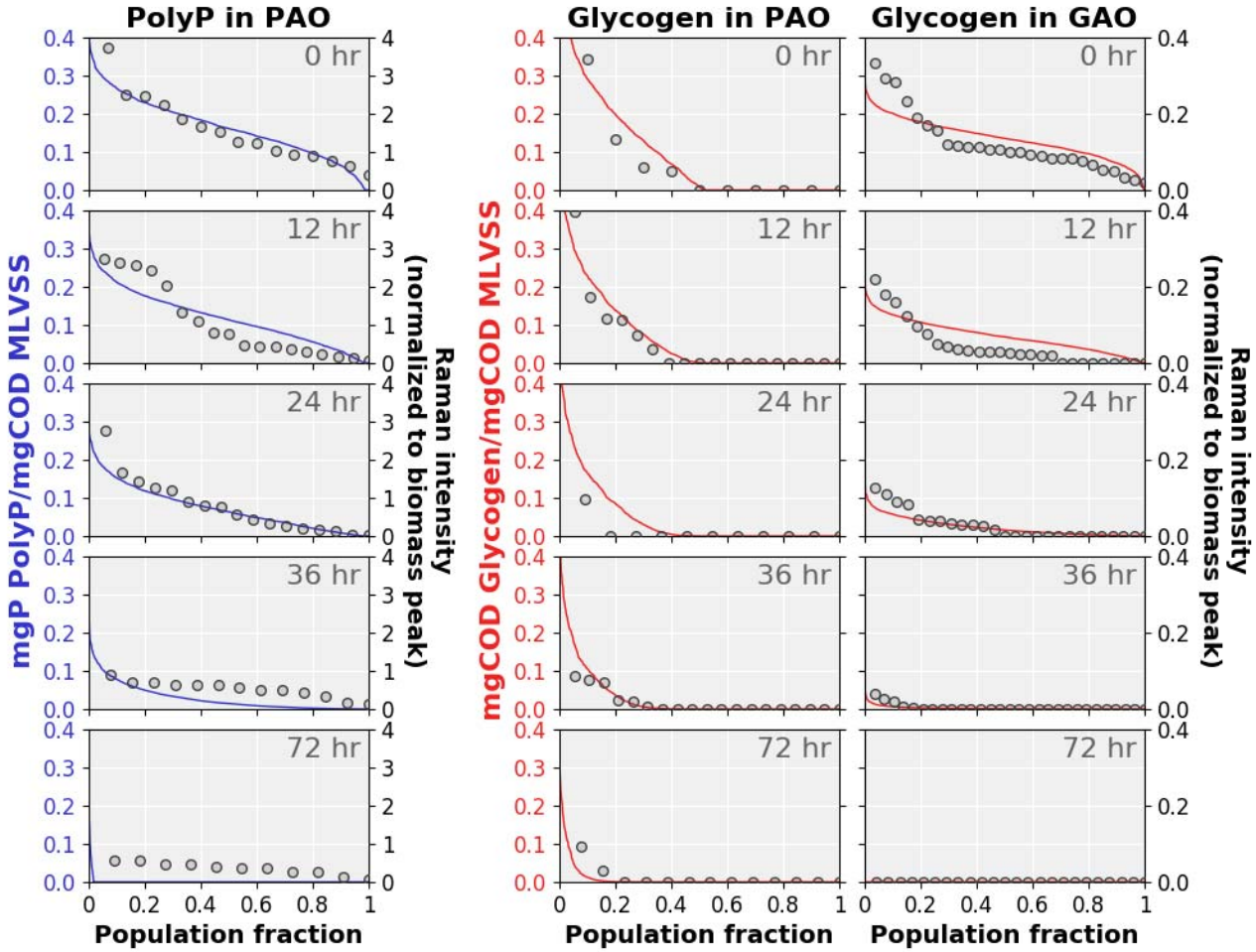

458 **Figure 4.** Comparison of model predicted polyP and glycogen dynamics in PAO and GAO cells with the observed

459 dynamics acquired by Raman single-cell micro-spectroscopy (dots) during a 72-hr anaerobic incubation batch

460 testing (this study). Tested sludge was sampled from a full-scale S2EBPR system (SSR configuration, South Cary

461 WRF, Apex, NC)

462

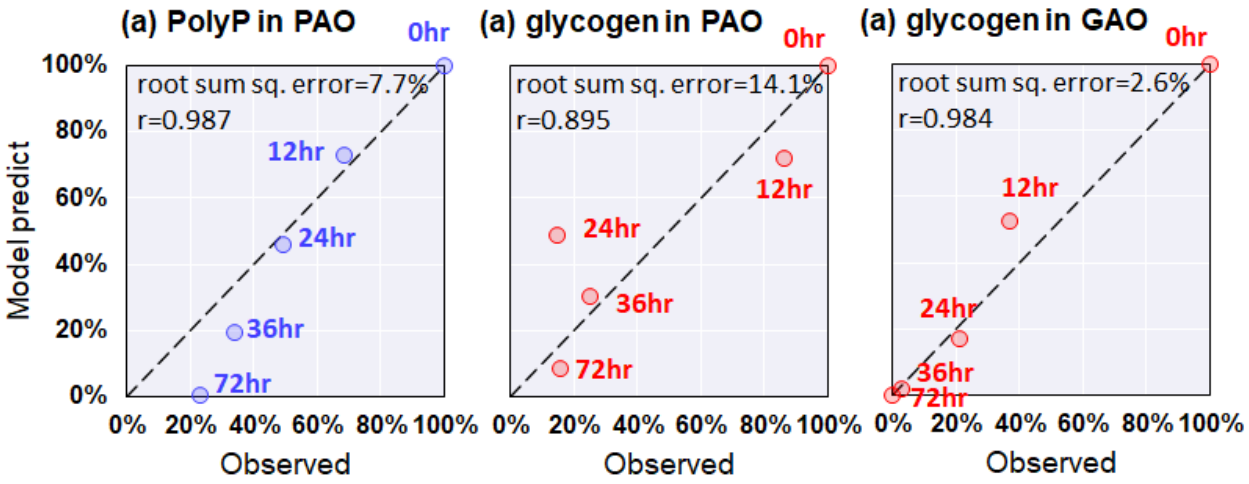

463

464 **Figure 5.** Comparison of model predicted polyP and glycogen dynamics in PAO and GAO cells with the observed

465 dynamics acquired by Raman single-cell micro-spectroscopy during a 72-hr anaerobic incubation batch testing (this

466 study). Polymer contents were normalized to their initial content at the beginning of this batch testing. Tested

467 sludge was sampled from a full-scale S2EBPR system (SSR configuration, South Cary WRF, Apex, NC).

468 ***PAO's competitive advantage with polymer utilization versatility.*** It was hypothesized that the

469 extended anaerobic condition and other factors in S2EBPR give PAOs more competitive advantages over

470 GAOs (Carvalheira et al., 2014; Tooker et al., 2017; Wang et al., 2019b) Our results suggested that PAO's

471 more versatile polymer storage and metabolism were probable contributing factors to this advantage.

472 **Figure 5** showed a glycogen depletion in GAO cells at around 36 hrs, with 97.2% of the initial storage

473 already consumed. GAOs, therefore, transitioned into the decay status earlier than PAO because
474 glycogen is the only energy source for their cell maintenance. In comparison, 33.9% of initial polyP and
475 25.3% of initial glycogen (19.3% and 30.3% as predicted by iEBPR respectively) were still available to
476 PAOs for cell maintenance at 36 hours, with ~92% and ~16% of PAO cells still had detectable
477 intracellular polyP and glycogen for cell maintenance as confirmed by the SCRS measurements. This
478 indicated that the majority of PAO cells remained in the cell maintenance phase rather than
479 transitioning into decay and lysis at 36 hrs. The model predicted ~1.6% cumulative GAO biomass loss, in
480 comparison to ~1.2% PAO biomass decay. The possession and ability of PAOs to sequentially use
481 multiple polymers enable its endurance to prolonged anaerobic conditions as shown in our study and
482 previous studies (Carvalheira et al., 2014; Onnis-Hayden et al., 2020a; Vargas et al., 2013) likely
483 contributed to PAOs' competitive advantage over GAOs under S2EBPR conditions.

484 ***Modeling glycolysis-TCA pathway switch and PAO phenotype relative abundances.*** iEBPR provides a
485 direct way to model, calibrate, and simulate the proportion of different PAO subphenotypes. Two PAO
486 subphenotypes were modeled in iEBPR, (1) the glycolysis-TCA switchable PAO phenotype which
487 switches to TCA-oriented metabolism and continues PHA synthesis when polyP is present, but glycogen
488 is depleted, and (2) the glycolysis-only phenotype which the PHA synthesis will cease and transition into
489 cell maintenance/decay when glycogen is depleted. The two subphenotypes coexist in iEBPR and by
490 calibrating the abundance parameter of respective phenotype agents we can explicitly investigate and
491 estimate the relative abundances of these two PAO subphenotypes within the activated sludge. Our
492 result showed a dominance of glycolysis-TCA switchable phenotype, being calibrated to be 98.5%. The
493 PHA accumulation would have been significantly less than the experiment observation when the cells
494 were assumed to be strictly glycolysis-dependent, especially after the depletion of glycogen (**Figure 6**),

495 in comparison to the calibrated fit when allowing glycolysis-TCA switching (**Figure 3**). This result agreed
496 with previous observations that S2EBPR conditions potentially favor such PAO subphenotypes indicated
497 by high anaerobic TCA cycle activity (Lanham et al., 2013). It is worth noting that iEBPR chose the C-W
498 model to represent the TCA-oriented metabolic stoichiometry. In reality, it is a much more complex
499 metabolic network composed of various shunts and branches (D Brdjanovic et al., 1998; He and
500 McMahon, 2011; Hesselmann et al., 2000; Martin et al., 2006; Schuler and Jenkins, 2003; Wilmes et al.,
501 2008; Yagci et al., 2003). A major challenge to modeling this complex metabolic network is to reliably
502 determine the relative contribution of reducing power from each shunt and branch, which requires
503 further elucidation by further experimental evidence.

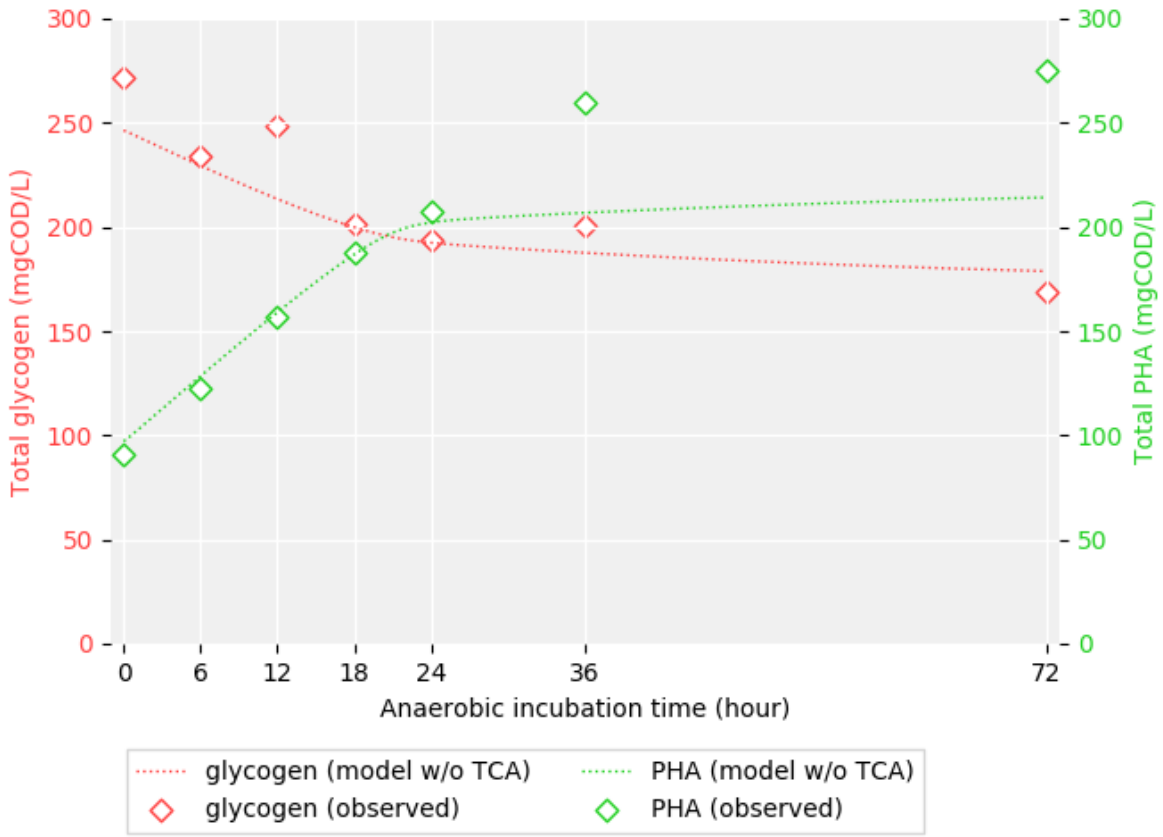

Figure 6. Modified iEBPR simulation restricting PAO cells to use glycolysis-only PHA synthesis resulted in significantly underpredicted PHA accumulation than observation. The tested activated sludge was sampled from a full-scale S2EBPR system (SSR configuration, South Cary WRF, Apex, NC), containing 6.9% as Accumulibacter-PAO, 1.1% as GAOs (estimated in biovolume by FISH). iEBPR incorporates three improved mechanisms: sequential polymer usage in cell maintenance, staged maintenance-decay, and PAO glycolysis-TCA pathway switch (disabled in this simulation), all designed for S2EBPR-like extended anaerobic incubations.

In addition, we acknowledge the limitations of iEBPR as an assessment tool to further resolve PAO phenotypes. First, non-Accumulibacter PAOs are not considered in iEBPR, such as the genus

514 *Tetrasphaera* which does not accumulate PHA anaerobically (Fernando et al., 2019; Kristiansen et al.,
515 2013). Therefore, we made the model framework expandable to incorporate new species in the future.
516 Second, iEBPR does not account for "inert" polyP content that is experimentally observed (Barker and
517 Dold, 1997). This could partially explain the remaining detectable polyP content persisted through the
518 entire 72-hr incubation period (**Figure 4**). Third, iEBPR highly relies on measurements at the single-cell
519 level resolution to accurately model the metabolic activity of an integrated microbial population.
520 Breakthroughs in SCRS-based polymer quantification methods were still in demand to improve detection
521 sensitivity and accuracy. Finally, competition on the substrates is the only modeled interaction between
522 agents in iEBPR. Other interactions, either mutualistic or competitive, intraspecies or interspecies, are
523 not considered in iEBPR but are common in the microbial ecology of activated sludge. More
524 sophisticated SCRS datasets are required to reveal their effects which are beyond the scope of this
525 study.

526

527 **CONCLUSION**

528 iEBPR, an agent-based model that incorporates the sequential polymer usage, staged maintenance-
529 decay processes, and glycolysis-TCA pathway shift, was developed, calibrated and validated using both
530 bulk batch test experimental data and high-resolution cellular and population-level measurements
531 enabled by SCRS.

532 • iEBPR improves the simulation accuracy on S2EBPR systems, where a longer anaerobic S2EBPR
533 SRT may lead to more pronounced PAO-GAO anaerobic competition mechanisms that differ
534 from those in play in conventional EBPR systems (e.g. A2O configuration).
535 • iEBPR revealed that under extended anaerobic conditions as in S2EBPR, the possession and
536 versatile ability of PAOs to sequentially use different intracellular polymers (glycogen and polyP)
537 as energy sources give them the competitive advantages over GAOs, as the results of longer
538 survival with longer maintenance state and later on-set of cell decay than GAOs that can only
539 utilize glycogen.
540 • iEBPR incorporates three newly proposed aspects, namely sequential polymer usage, staged
541 maintenance-decay processes, and glycolysis-TCA pathway switch, which allows more accurate
542 and higher-resolved simulation of the competition between PAO subphenotypes under
543 anaerobic conditions.
544 • The combination of the agent-based model of coexistence of PAO subphenotypes of key
545 populations and, SCRS-resolved intracellular polymer quantification allowed experimental
546 verification of the proposed metabolic mechanisms at both population and cell group levels in
547 activated sludge.
548 • iEBPR can be applied to facilitate and optimize the design and operations of S2EBPR for
549 improved simulations of nutrient removal and recovery from wastewater.

550 Further studies are still in demand to improve iEBPR, including non-Accumulibacter PAOs, nitrogen-
551 related metabolism and organisms, and modeling more diverse and comprehensive biological
552 interactions between organisms.

553

ACKNOWLEDGMENT

This work was supported by the Water Environment Research Foundation (Grant No. U1R13) and funds from Hampton Roads Sanitation District and Woodard & Curran, Inc. Special thanks to Clean Water Services and the South Cary Water Reclamation Facility operators and staff, and the entire WEF (previously WERF) S2EBPR Project Team for their generous support and assistance throughout the study.

REFERENCES

Acevedo B, Oehmen A, Carvalho G, Seco A, Borrás L, Barat R. Metabolic shift of polyphosphate-accumulating organisms with different levels of polyphosphate storage. Water Res 2012;46:1889–900. https://doi.org/10.1016/j.watres.2012.01.003.

Barker P, Dold P. General model for biological nutrient removal activated-sludge systems: model presentation. Water Environ Res 1997;69:969–84.

Barnard J, Houweling D, Analla H, Steichen M. Fermentation of mixed liquor for phosphorus removal. Proc Water Environ Fed 2010;2010:59–71.

Brdjanovic Damir, van Loosdrecht MC, Hooijmans CM, Mino T, Alaerts GJ, Heijnen JJ. Bioassay for glycogen determination in biological phosphorus removal systems. Water Sci Technol 1998;37:541–7.

Brdjanovic D, Van Loosdrecht M, Hooijmans C, Mino T, Alaerts G, Heijnen J. Effect of polyphosphate limitation on the anaerobic metabolism of phosphorus-accumulating microorganisms. Appl Microbiol Biotechnol 1998;50:273–6.

Bucci V, Majed N, Hellweger FL, Gu AZ. Heterogeneity of intracellular polymer storage states in enhanced biological phosphorus removal (EBPR)–observation and modeling. Environ Sci Technol 2012;46:3244–52.

Carvalheira M, Oehmen A, Carvalho G, Reis MA. Survival strategies of polyphosphate accumulating organisms and glycogen accumulating organisms under conditions of low organic loading. Bioresour Technol 2014;172:290–6.

581 Comeau Y, Hall K, Hancock R, Oldham W. Biochemical model for enhanced biological phosphorus
582 removal. Water Res 1986;20:1511–21.

583 Copp JB, Belk I, Vale P. Operational control of a RAS fermentation process for enhancing biological
584 phosphorus removal. Proc Water Environ Fed 2012;2012:6056–68.

585 Dunlap P, Martin K, Stevens G, Tooker N, Barnard J, Gu A, et al. Rethinking EBPR: What Do You Do When
586 the Model Will Not Fit Real-World Evidence? 5th IWA. WEF Wastewater Treat. Model. Semin.
587 Annecy Fr., 2016, p. 39–62.

588 Fernando EY, McIlroy SJ, Nierychlo M, Herbst F-A, Petriglieri F, Schmid MC, et al. Resolving the individual
589 contribution of key microbial populations to enhanced biological phosphorus removal with
590 Raman–FISH. ISME J 2019;13:1933–46.

591 Filipe CD, Daigger GT, Grady C. Effects of pH on the rates of aerobic metabolism of phosphate-
592 accumulating and glycogen-accumulating organisms. Water Environ Res 2001a;73:213–22.

593 Filipe CD, Daigger GT, Grady C. A metabolic model for acetate uptake under anaerobic conditions by
594 glycogen accumulating organisms: stoichiometry, kinetics, and the effect of pH. Biotechnol Bioeng
595 2001b;76:17–31.

596 Gu AZ, Saunders A, Neethling J, Stensel H, Blackall L. Functionally relevant microorganisms to enhanced
597 biological phosphorus removal performance at full-scale wastewater treatment plants in the
598 United States. Water Environ Res 2008;80:688–98.

599 Gu AZ, Tooker NB, Onnis-Hayden A, Wang D, Li G, Srinivasan V, et al. Investigation of the Mechanisms
600 for Optimization and Design of a Side-Stream EBPR Process as a Sustainable Approach for
601 Achieving Stable and Efficient Phosphorus Removal. Water Research Foundation (WRF); 2018.
602 ISBN:978-1-60573-351-7. WRF Project Number: U1R13/4859.

603 Guedes da Silva L, Olavarria Gamez K, Castro Gomes J, Akkermans K, Welles L, Abbas B, et al. Revealing
604 the metabolic flexibility of “Candidatus Accumulibacter phosphatis” through redox cofactor
605 analysis and metabolic network modeling. Appl Environ Microbiol 2020;86:e00808-20.

606 Gujer W. The Activated Sludge Model No. 2: Biological Phosphorus Removal: Proceedings IAWQ
607 Specialised Seminar: Modelling and Control of Activated Sludge Processes, 22.-24. August 1994,
608 Copenhagen. IAWQ; 1994.

609 He S, McMahon KD. ‘Candidatus Accumulibacter’gene expression in response to dynamic EBPR
610 conditions. ISME J 2011;5:329.

611 Henze M, Harremoes P, la Cour Jansen J, Arvin E. Wastewater treatment: biological and chemical
612 processes. Springer Science & Business Media; 2001.

613 Hesselmann R, Von Rummell R, Resnick SM, Hany R, Zehnder A. Anaerobic metabolism of bacteria
614 performing enhanced biological phosphate removal. Water Res 2000;34:3487–94.

615 Houweling D, Comeau Y, Takács I, Dold P. Uncertainty and variability in enhanced biological phosphorus
616 removal (EBPR) stoichiometry: consequences for process modelling and optimization. Water Sci
617 Technol 2010;61:1793–800.

618 Hu Z, Wentzel M, Ekama G. A general kinetic model for biological nutrient removal activated sludge
619 systems: Model development. Biotechnol Bioeng 2007;98:1242–58.

620 Kristiansen R, Nguyen HTT, Saunders AM, Nielsen JL, Wimmer R, Le VQ, et al. A metabolic model for
621 members of the genus Tetrasphaera involved in enhanced biological phosphorus removal. ISME J
622 2013;7:543.

623 Kurve A, Kotobi K, Kesidis G. An agent-based framework for performance modeling of an optimistic
624 parallel discrete event simulator. Complex Adapt Syst Model 2013;1:1–24.

625 Lanham AB, Oehmen A, Saunders AM, Carvalho G, Nielsen PH, Reis MA. Metabolic modelling of full-
626 scale enhanced biological phosphorus removal sludge. Water Res 2014;66:283–95.

627 Lanham AB, Oehmen A, Saunders AM, Carvalho G, Nielsen PH, Reis MA. Metabolic versatility in full-scale
628 wastewater treatment plants performing enhanced biological phosphorus removal. Water Res
629 2013;47:7032–41.

630 Li G, Tooker NB, Wang D, Srinivasan V, Barnard JL, Schauer P, et al. Application of Agent-Based Modeling
631 to Reveal Competition between PAOs and GAOs in Side-Stream EBPR (S2EBPR) Systems. Proc
632 Water Environ Fed 2018;2018:269–74.

633 Li G, Tooker NB, Wang D, Srinivasan V, Onnis-Hayden A, Barnard JL, et al. Modeling Side-stream
634 Enhanced Biological Phosphorus Removal (S2EBPR) Systems: Insights from versatile anaerobic
635 pathways. Proc Water Environ Fed 2020.

636 Li Y, Cope HA, Rahman SM, Li G, Nielsen PH, Elfick A, et al. Toward Better Understanding of EBPR
637 Systems via Linking Raman-Based Phenotypic Profiling with Phylogenetic Diversity. Environ Sci
638 Technol 2018;52:8596–606.

639 Lopez C, Pons M, Morgenroth E. Endogenous processes during long-term starvation in activated sludge
640 performing enhanced biological phosphorus removal. Water Res 2006;40:1519–30.

641 López-V CM, Hooijmans CM, Brdjanovic D, Gijzen HJ, van Loosdrecht MC, others. Occurrence of glycogen
642 accumulating organisms (GAO) at full-scale enhanced biological phosphorus removal (EBPR)
643 wastewater treatment plants. Nutr. Remov. Recovery Symp. 2007, Water Environment Federation;
644 2007, p. 968–89.

645 Lopez-Vazquez CM, Oehmen A, Hooijmans CM, Brdjanovic D, Gijzen HJ, Yuan Z, et al. Modeling the PAO–
646 GAO competition: effects of carbon source, pH and temperature. Water Res 2009;43:450–62.

647 Lu H, Keller J, Yuan Z. Endogenous metabolism of Candidatus Accumulibacter phosphatis under various
648 starvation conditions. Water Res 2007;41:4646–56.

649 Majed N, Gu AZ. Phenotypic dynamics in polyphosphate and glycogen accumulating organisms in
650 response to varying influent C/P ratios in EBPR systems. Sci Total Environ 2020;743:140603.

651 Majed N, Gu AZ. Insights into the Metabolic Pathways and Diversity of Functionally Relevant Populations
652 in Enhanced Biological Phosphorus Removal Processes using Raman Microscopy. Proc Water
653 Environ Fed 2011;2011:4824–32.

654 Majed N, Gu AZ. Application of Raman microscopy for simultaneous and quantitative evaluation of
655 multiple intracellular polymers dynamics functionally relevant to enhanced biological phosphorus
656 removal processes. Environ Sci Technol 2010;44:8601–8.

657 Majed N, Matthäus C, Diem M, Gu AZ. Evaluation of intracellular polyphosphate dynamics in enhanced
658 biological phosphorus removal process using Raman microscopy. Environ Sci Technol
659 2009;43:5436–42.

660 Martin HG, Ivanova N, Kunin V, Warnecke F, Barry KW, McHardy AC, et al. Metagenomic analysis of two
661 enhanced biological phosphorus removal (EBPR) sludge communities. Nat Biotechnol
662 2006;24:1263–9.

663 Maurer M, Gujer W, Hany R, Bachmann S. Intracellular carbon flow in phosphorus accumulating
664 organisms from activated sludge systems. Water Res 1997;31:907–17.

665 Mielczarek AT, Nguyen HTT, Nielsen JL, Nielsen PH. Population dynamics of bacteria involved in
666 enhanced biological phosphorus removal in Danish wastewater treatment plants. Water Res
667 2013;47:1529–44.

668 Mino T, Arun V, Tsuzuki Y, Matsuo T. Effect of phosphorus accumulation on acetate metabolism in the
669 biological phosphorus removal process. Biol. Phosphate Remov. Wastewaters, Elsevier; 1987, p.
670 27–38.

671 Mino T, Van Loosdrecht M, Heijnen J. Microbiology and biochemistry of the enhanced biological
672 phosphate removal process. Water Res 1998;32:3193–207.

673 Neethling J, Bakke B, Benisch M, Gu A, Stephens H, Stensel HD, et al. Factors influencing the reliability of
674 enhanced biological phosphorus removal. Water Environment Research Foundation; 2006.

675 Nielsen PH, McIlroy SJ, Albertsen M, Nierychlo M. Re-evaluating the microbiology of the enhanced
676 biological phosphorus removal process. Curr Opin Biotechnol 2019;57:111–8.

677 Nielsen PH, Vollertsen J, Sørensen KH. Method and a system for out-competing glycogen-accumulating
678 organisms in a substance. Google Patents; 2016.

679 Oehmen A, Lemos PC, Carvalho G, Yuan Z, Keller J, Blackall LL, et al. Advances in enhanced biological
680 phosphorus removal: from micro to macro scale. Water Res 2007;41:2271–300.

681 Oehmen A, Vives MT, Lu H, Yuan Z, Keller J. The effect of pH on the competition between
682 polyphosphate-accumulating organisms and glycogen-accumulating organisms. Water Res
683 2005a;39:3727–37.

684 Oehmen A, Yuan Z, Blackall LL, Keller J. Comparison of acetate and propionate uptake by polyphosphate
685 accumulating organisms and glycogen accumulating organisms. Biotechnol Bioeng 2005b;91:162–
686 8.

687 Oehmen A, Zeng RJ, Saunders AM, Blackall LL, Keller J, Yuan Z. Anaerobic and aerobic metabolism of
688 glycogen-accumulating organisms selected with propionate as the sole carbon source.
689 Microbiology 2006;152:2767–78.

690 Onnis-Hayden A, Majed N, Li Y, Rahman SM, Drury D, Risso L, et al. Impact of solid residence time (SRT)
691 on functionally relevant microbial populations and performance in full-scale enhanced biological
692 phosphorus removal (EBPR) systems. Water Environ Res 2020a;92:389–402.

693 Onnis-Hayden A, Srinivasan V, Tooker NB, Li G, Wang D, Barnard JL, et al. Survey of full-scale sidestream
694 enhanced biological phosphorus removal (S2EBPR) systems and comparison with conventional
695 EBPRs in North America: Process stability, kinetics, and microbial populations. Water Environ Res
696 2020b;92:403–17. https://doi.org/10.1002/wer.1198.

697 Pereira H, Lemos PC, Reis MA, Crespo JP, Carrondo MJ, Santos H. Model for carbon metabolism in
698 biological phosphorus removal processes based on in vivo13C-NMR labelling experiments. Water
699 Res 1996;30:2128–38.

700 Pijuan M, Oehmen A, Baeza JA, Casas C, Yuan Z. Characterizing the biochemical activity of full-scale
701 enhanced biological phosphorus removal systems: a comparison with metabolic models.
702 Biotechnol Bioeng 2008;99:170–9.

703 Rodrigo M, Seco A, Penya-Roja J, Ferrer J. Influence of sludge age on enhanced phosphorus removal in
704 biological systems. Water Sci Technol 1996;34:41–8.

705 Santos JM, Rieger L, Lanham AB, Carvalheira M, Reis MA, Oehmen A. A novel metabolic-ASM model for
706 full-scale biological nutrient removal systems. Water Res 2020;171:115373.

707 Schuler AJ, Jenkins D. Enhanced biological phosphorus removal from wastewater by biomass with
708 different phosphorus contents, part III: anaerobic sources of reducing equivalents. Water Environ
709 Res 2003;75:512–22.

710 Smolders G, Klop J, Van Loosdrecht M, Heijnen J. A metabolic model of the biological phosphorus
711 removal process: I. Effect of the sludge retention time. Biotechnol Bioeng 1995;48:222–33.

712 Smolders G, Van der Meij J, Van Loosdrecht M, Heijnen J. Model of the anaerobic metabolism of the
713 biological phosphorus removal process: stoichiometry and pH influence. Biotechnol Bioeng
714 1994a;43:461–70.

715 Smolders G, Van der Meij J, Van Loosdrecht M, Heijnen J. Stoichiometric model of the aerobic
716 metabolism of the biological phosphorus removal process. Biotechnol Bioeng 1994b;44:837–48.

717 Srinivasan VN, Li G, Wang D, Tooker NB, Dai Z, Onnis-Hayden A, et al. Oligotyping and metagenomics
718 reveal distinct Candidatus Accumulibacter communities in side-stream versus conventional full-
719 scale enhanced biological phosphorus removal (EBPR) systems. Water Res 2021;206:117725.

720 Stevens G, Ellsworth A, Wyman M, Lambrecht A. BNR process using RAS anaerobic zone. Proc Water
721 Environ Fed 2015;2015:1–3.

722 Stokholm-Bjerregaard M, McIlroy SJ, Nierychlo M, Karst SM, Albertsen M, Nielsen PH. A critical
723 assessment of the microorganisms proposed to be important to enhanced biological phosphorus
724 removal in full-scale wastewater treatment systems. Front Microbiol 2017;8:718.

725 Stroud R, Martin C. South Cary Water Reclamation Facility's Nutrient Removal Modifications and
726 Reduction Success, Town of Cary, North Carolina. Proc Water Environ Fed 2001;2001:337–45.

727 Tooker NB, Li G, Bott C, Dombrowski P, Schauer P, Menniti A, et al. Rethinking and reforming enhanced
728 biological phosphorus removal (EBPR) strategy–concepts and mechanisms of side-stream EBPR.
729 WEFTEC 2017, Water Environment Federation; 2017.

730 Vale P, Barnard J, Thomas D, Dold P. RAS fermentation to enhance biological phosphorus removal. Proc.
731 WEFTEC Conf., 2008.

732 Vargas M, Yuan Z, Pijuan M. Effect of long-term starvation conditions on polyphosphate-and glycogen-
733 accumulating organisms. Bioresour Technol 2013;127:126–31.

734 Vollertsen J, Petersen G, Borregaard VR. Hydrolysis and fermentation of activated sludge to enhance
735 biological phosphorus removal. Water Sci Technol 2006;53:55–64.

736 Wang D, Tooker NB, Li G, Srinivasan V, Onnis-Hayden A, Gu AZ. Single-cell Raman spectroscopy-based
737 phenotyping revealed metabolic difference between side-stream and conventional enhanced
738 biological phosphorus removal systems, 2019a.

739 Wang D, Tooker NB, Srinivasan V, Li G, Fernandez LA, Schauer P, et al. Side-stream enhanced biological
740 phosphorus removal (S2EBPR) process improves system performance - A full-scale comparative
741 study. Water Res 2019b;167:115109. https://doi.org/10.1016/j.watres.2019.115109.

742 Wentzel M, Dold P, Ekama G, Marais G. Enhanced polyphosphate organism cultures in activated sludge
743 systems. Part III: Kinetic model. Water A 1989;15:89–102.

744 Whang L-M, Filipe C, Park J. Model-based evaluation of competition between polyphosphate-and
745 glycogen-accumulating organisms. Water Res 2007;41:1312–24.

746 Wilmes P, Wexler M, Bond PL. Metaproteomics provides functional insight into activated sludge
747 wastewater treatment. PLoS One 2008;3:e1778.

748 Yagci N, Artan N, Çokgör EU, Randall CW, Orhon D. Metabolic model for acetate uptake by a mixed
749 culture of phosphate-and glycogen-accumulating organisms under anaerobic conditions.
750 Biotechnol Bioeng 2003;84:359–73.

751 Zeng RJ, van Loosdrecht M, Yuan Z, Keller J. Metabolic model for glycogen-accumulating organisms in
752 anaerobic/aerobic activated sludge systems. Biotechnol Bioeng 2003;81:92–105.

753 Zhou Y, Pijuan M, Zeng RJ, Yuan Z. Involvement of the TCA cycle in the anaerobic metabolism of
754 polyphosphate accumulating organisms (PAOs). Water Res 2009;43:1330–40.

755